Preparation and Characterization of $Cu_2ZnSn(S_xSe_{1-x})_4$ Thin Films by Synchronous Sulfo-Selenization of Single-Source Evaporated Metallic Precursors

Xin Jiang · Lexi Shao · Jun Zhang · Jianmin Chen

Abstract $Cu_2ZnSn(S,Se)_4$ (CZTSSe) thin film was prepared using a simple two-step approach based on the single-source evaporation and synchronous sulfo-selenization. Composition, microstructure, morphology, and properties of the as-prepared CZTSSe thin films were investigated. XRD and Raman patterns confirmed the formation of single-phase CZTSSe solid solutions. SEM results showed that the CZTSSe thin film had a uniform morphology and large grains. EDS results revealed the composition of CZTSSe film was Cu:Zn:Sn:S:Se = 23.7:12.6:12.2:37.7:13.8 (in at%), which was in accordance with the stoichiometric $Cu_2ZnSn(S,Se)_4$. The optical band gap of CZTSSe thin film evaluated from its UV–Vis spectrum was 1.33 eV. The resistivity, carrier concentration, and mobility were 0.53 Ω cm, 7.9×10^{18} cm^3, and 7.5 cm^2/(Vs), respectively.

KEY WORDS: $Cu_2ZnSn(S,Se)_4$; Evaporation; Sulfo-selenization; Thin film

1 Introduction

Chalcogenide kesterites Cu_2ZnSnS_4(CZTS) thin film is a promising candidate for the next-generation thin film solar cells due to its excellent optical and electrical properties [1, 2], and it contains only abundant and non-toxic elements [3]. The incorporation of Se into CZTS can tune the optical band gap of the $Cu_2ZnSn(S,Se)_4$(CZTSSe) alloy by varying

X. Jiang · J. Chen (✉)
State Key Laboratory of Solid Lubrication, Lanzhou Institute of Chemical Physics, Chinese Academy of Sciences, Lanzhou 730000, China
e-mail: chenjm@licp.cas.cn

X. Jiang · L. Shao · J. Zhang
School of Physical Science and Technology, Zhanjiang Normal University, Zhanjiang 524048, China

X. Jiang
University of Chinese Academy of Sciences, Beijing 100049, China

the Se/S ratio. Currently, CZTSSe-based solar cells have achieved the conversion efficiency beyond 11% [4], which is higher than that of quaternary CZTS solar cells. So far, many vacuum- and non-vacuum-based methods have been developed to prepare the CZTSSe films and devices, including solid-state reaction [5], evaporation [6, 7], sputtering [8], pulsed-laser deposition [9], monograin synthesis [10], ink-based approaches [4, 11, 12], and so on. In terms of large-scale preparation, vacuum-based techniques seem to be more promising. Vacuum-based method preparing CZTSSe thin films consists of two steps [6–8]. Firstly, a precursor containing sulfur or selenium is deposited by multi-source vacuum deposition techniques (evaporation or sputtering). Secondly, the precursor is submitted to a reactive annealing step under an atmosphere containing the alternate chalcogenide element to form the desired film. Metal sulfides or selenides are usually employed as source materials to supply the sulfur or selenium for precursor in the first step. The composition of the precursor is controlled by the thickness of stacked element layer [7] or the deposition rate of each source [8]. In this case, complex deposition system and monitoring equipments, such as multi-

effusion cells, multi-target, deposition rate monitor, and thickness monitor, are necessary, which goes against the reduce of equipment cost. Moreover, how to precisely tune the contents of sulfur and selenium introduced in different steps is a challenge. Another potential method to prepare the CZTSSe thin film is to deposit the pure metallic precursor by evaporation or sputtering, and the following reactive annealing step is treated in two stages, starting with a sulfurization stage followed by a selenization stage, or vice versa. Nevertheless, two-step annealing complicates the annealing installment and processing, which would consume a great deal of time and energy. Thus, a single-step annealing process by which metallic precursor could be sulfurized and selenized simultaneously is of great interest [13–15].

A simple two-step method which combined the single-source evaporation and synchronous sulfo-selenization was developed to prepare CZTSSe thin film. Compared with the approaches based on multi-source deposition and two-step reactive annealing, this method significantly simplifies the equipments and processes and reduces the cost. The composition, microstructure, morphology, optical, and electrical properties of as-synthesized CZTSSe thin films were investigated.

2 Experimental

The CZTSSe thin films were prepared by a two-step approach. Firstly, precursors were deposited by the thermal evaporation system with a single-source consisting of Cu patch, Zn, and Sn powder. Cu, Zn, and Sn were deposited on a Mo-coated soda lime glass substrate (Mo-coated SLG) simultaneously. Then, the precursors were annealed in the mixed atmosphere of sulfur (S) and selenium (Se) confined in a graphite boat chamber of the electric furnace to obtain CZTSSe films. Before depositing the precursors, the substrates were thoroughly cleaned with organic solvents and deionized water. The background pressure of the evaporation chamber was evacuated below 1×10^{-3} Pa with a rotary mechanical pump and a diffused pump. The metallic mixtures of Cu, Sn, and Zn (purity 99.99%) were used as the evaporation sources. The pressure was maintained at 2×10^{-3} Pa during evaporation. The thicknesses of the precursors could be well adjusted by the mass of evaporation sources. After depositing, the precursors were immediately transferred to a graphite boat containing equivalent amount of S and Se powers (purity 99.99%) in the electric furnace for sulfo-selenization. The heating and cooling followed the same procedure described in previous work [16].

To reduce the loss of Sn in the precursors during the annealing process, the composition of evaporation sources was designed to be Sn-rich with a ratio of Zn/Sn = 0.83. The chemical composition of evaporation sources is listed in Table 1. In addition, in order to evaluate the optical and electrical properties, the samples were also deposited on the soda lime glass substrate (SLG) under the same conditions.

The structural quality of the samples was examined using X-ray diffraction (XRD, Bruker AXSD8 Advance) with a CuK_α radiation source ($\lambda = 488$ nm). Raman scattering measurements were performed with a confocal Raman spectrometer (Renishaw inVia micro-Raman system) excited by Ar^+ laser with wavelength of 532 nm. The composition and morphology of the thin film were characterized by energy-dispersive spectroscopy (EDS, Hitachi S4800) and scanning electron microscopy (SEM, Hitachi S4800). The optical and electrical properties were analyzed by UV–Vis spectrophotometer (Perkin-Elmer Lambda 950) and Hall measurements (UK Accent HL5500PC), respectively.

3 Results and Discussion

The chemical compositions deduced from EDS measurements are shown in Table 1. The composition of evaporation source was set to Cu-poor and Zn-poor. As it is shown in Table 1, the composition of the precursor is close to that of evaporation source, which indicated that the metal materials in evaporation source were exhausted and transferred proportionally to the substrate during the evaporation. In comparison to the precursor, the element ratios of Cu/(Zn + Sn) and Zn/Sn for CZTSSe film were both increased after annealed in Sulfur and Selenium mixed atmosphere. This is due to the Sn losses through desorption of SnS(Se) from CZTSSe film at elevated temperature [17]. Moreover, the possibility of the re-evaporation of Zn from the CZTSSe thin film should not be excluded.

Figure 1 shows the EDS spectrum of CZTSSe thin films. The chemical composition ratio of CZTSSe thin films was Cu:Zn:Sn:S:Se = 23.7:12.6:12.2:37.7:13.8 (in at%), which is consistent with the stoichiometry of $Cu_2ZnSn(S_xSe_{1-x})_4$ despite slightly Cu-poor. Cu-poor composition can effectively avoid the formation of Cu sulfide or selenide, which is detrimental to the performance of solar cells. The ratio of S:Se was about 2.7:1, lower Se concentration was due to the lower vapor pressure of Se compared with that of S.

Figures 2 and 3 show the XRD patterns of the Cu–Zn–Sn precursor and CZTSSe thin film coated onto the Mo-coated glass substrate. The XRD diffraction peaks corresponding to Sn (JCPDS 04-0673), $Cu_{41}Sn_{11}$ (JCPDS 30-0510), CuZn (JCPDS 08-0349), Cu_6Sn_5 (JCPDS 45-1488), and (Cu,Sn) (JCPDS 06-0621) phases were

Table 1 Chemical compositions of the evaporation source, precursor, and CZTSSe thin film

Name	Composition (at%)					Ratio of composition			
	Cu	Zn	Sn	S	Se	Cu/(Zn + Sn)	Zn/Sn	Metal/(S + Se)	S/Se
Evaporation source	45	25	30	–	–	0.82	0.83	–	–
Precursor	46.1	24.6	29.3	–	–	0.86	0.84	–	–
CZTSSe	23.7	12.6	12.2	37.7	13.8	0.95	1.03	0.94	2.73
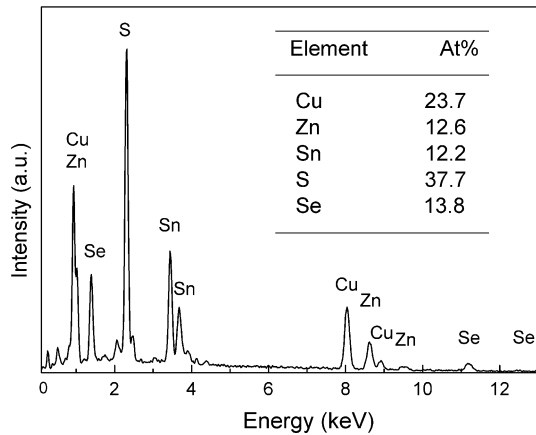
Fig. 1 EDS spectrum of CZTSSe thin film
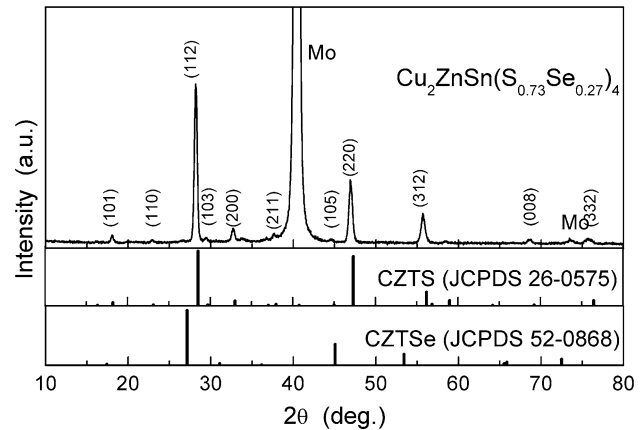
Fig. 3 XRD pattern of CZTSSe thin film
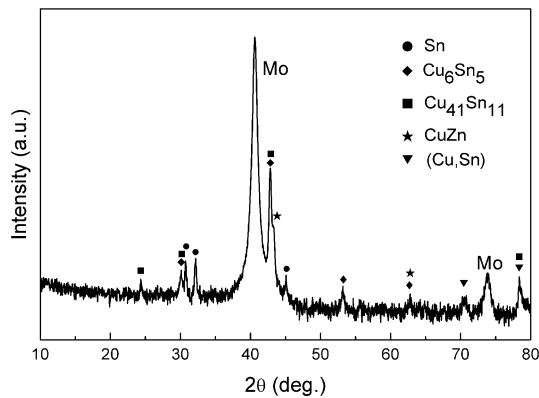
Fig. 2 XRD pattern of Cu–Zn–Sn precursor
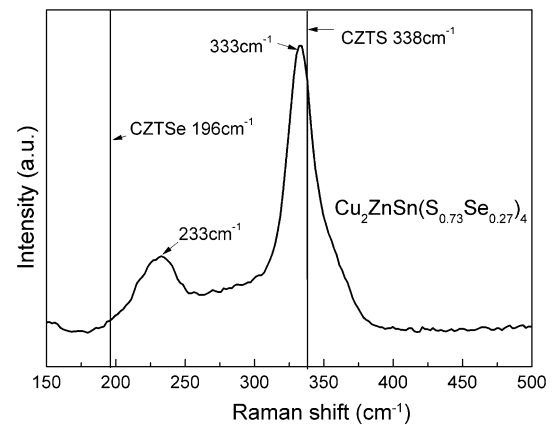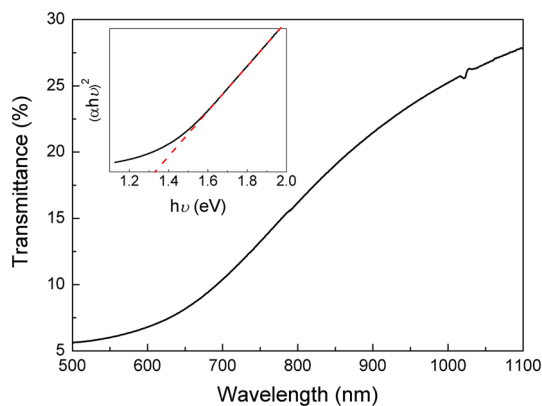

Fig. 4 Raman spectrum of CZTSSe thin film

observed in the Cu–Zn–Sn precursors besides Mo. The absence of peaks for Cu element and ternary phase indicates that Cu was inclined to react with Zn or Sn to form a Cu binary phase rather than a ternary Cu–Zn–Sn alloy. This is in agreement with the result reported by Kim et al. [18]. The lower intensity for some peaks can attribute to the poor crystallinity of alloying precursor. After annealing the Cu–Zn–Sn precursor in the mixed atmosphere of S and Se, the obtained CZTSSe thin film had the diffraction pattern similar to that of CZTS with a tetragonal crystal structure. However, all the peaks moved to lower diffraction angles

in comparison with standard ones of CZTS (JCPDS 26-0575). This was because large Se atoms replaced partly small S atoms in the CZTSSe lattice resulting in the expansion of lattice.

The position of (112) peak for CZTSSe was at $2\theta = 28.17°$, which was between the (112) peaks for CZTSe and for CZTS. According to Ref. [7], the position of (112) peak can be used to estimate the ratio of S/(S + Se) supposing that the shift of the CZTSSe (112)
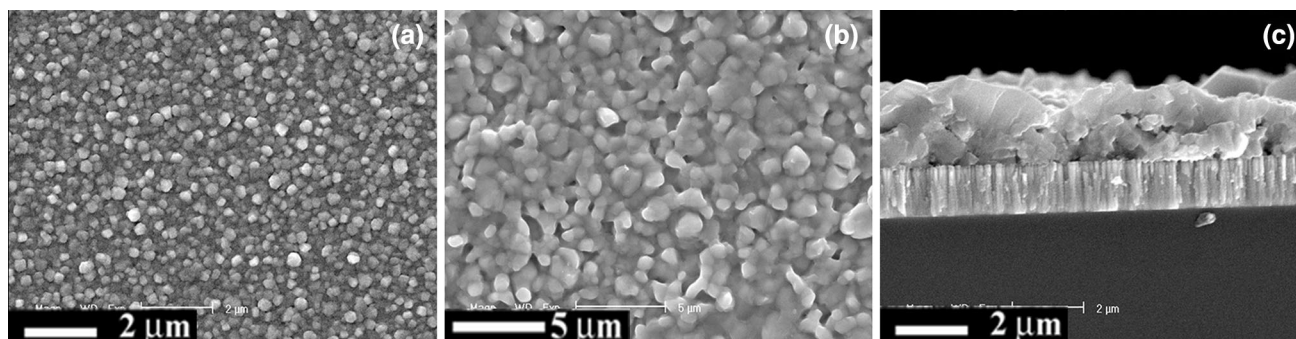
Fig. 5 SEM images of the top view for Cu–Zn–Sn precursor **a**, top view for CZTSSe thin film **b**, cross-sectional view for CZTSSe thin film **c**

Fig. 6 UV–Vis transmittance spectrum of CZTSSe thin film. The *inset* image shows the estimated band gap of 1.33 eV

peak follows a linear trend between the ones of CZTSe and CZTS. The relation between the position of (112) peak and the ratio of $[S]/([S] + [Se])$ can be expressed as $[S]/([S] + [Se]) = (x - 27.14)/A$, where A is a linear factor and takes the value 1.39, which results from the difference between the CZTS and CZTSe. With this equation, it was obtained that $[S]/([S] + [Se]) = 0.74$ for CZTSSe sample, which was in good agreement with EDS results. In addition, no peaks of other phases were observed in the CZTSSe pattern, which suggested pure CZTSSe phase may be obtained. Raman scattering was used to further analysis the structure and phase purity of the CZTSSe thin film. In Fig. 4, the Raman spectrum of CZTSSe sample is presented, and the literature values for the main peak positions of CZTSe and CZTS are represented as vertical lines. The Raman spectrum of CZTSSe sample exhibited a two-mode behavior due to the coexistence of S and Se atoms in sample. Two Raman peaks at 333 and 233 cm^{-1} corresponded to the A$_1$ modes of CZTS and CZTSe, respectively. However, the CZTS A$_1$ mode appeared to shift to the lower frequency direction, while the CZTSe A$_1$ mode shifted to the higher frequency direction compared with the standard peak positions. This

phenomenon can be explained by the mass effect and the change of the bond strength [5]. According to the extended model proposed by Keating et al. [19], the frequency of the A$_1$ mode decreased with increasing atomic mass and bond length. For one thing, Se atoms had larger atomic mass than S atoms, for another, according to the XRD analysis above, the incorporation of Se with large atomic radius can cause the expansion of lattice, indicating that the bond distance was lengthened. Thus, above two reasons determined the CZTS A$_1$ mode of CZTSSe solid solutions shift to lower frequency when Se atoms replaced partly S atoms. For CZTSe A$_1$ mode, the situation was reversed. Moreover, there were no obvious additional peaks in Raman spectrum suggesting the absence of impurities phase.

Figure 5 shows the SEM images of Cu–Zn–Sn precursor and CZTSSe thin film. The surface of the precursor showed a uniform distribution of small grains with well-defined boundaries. The grain size was about 300 nm. However, the morphology of evaporated precursor was not as compact as that prepared by sputtering [18]. This is because the sputtering process can provide stronger kinetic energy and migration ability for sputtered particles than thermal evaporation process, which was beneficial to form compact films. However, loose microstructure for our precursor was helpful for the diffusion of S and Se and promoted the complete reaction with alloy precursor. After sulfo-selenization, the grain size of CZTSSe thin film was obviously improved as shown in Fig. 5b. The CZTSSe thin film exhibited less well-defined crystallites with a size of 1 micron as well as some holes. A cross-sectional SEM image (Fig. 5c) showed that the CZTSSe thin film was approximately 1.5 μm thick, composed mainly of large grains.

Figure 6 shows the UV–Vis transmittance spectrum of the CZTSSe thin films prepared onto the glass substrate. The absorption coefficient of the sample (α) was derived from the transmittance data, which was larger than 10^4 cm^{-1} in the visible region. As shown in the inset, the optical band gap of the CZTSSe thin film was deduced

X. Jiang et al.: Acta Metall. Sin. (Engl. Lett.), 2014, **27**(4), 689–693

693

from the plot of $(\alpha h v)^2$ versus hv by extrapolating the straight line portion of the curve to the x-axis, where α is the absorption coefficient and hv is the photon energy. The optical band gap was estimated to be 1.33 eV, which was larger than that of CZTSe (1.0 eV) yet less than that of CZTS (1.5 eV). The band gap of CZTSSe was strongly dependent on the composition of the thin film. According to Ref. [20], the band gap E_g of CZTSSe thin film can be described by the following equation: $E_{g-\text{CZTSSe}} = yE_{g-\text{CZTSSe}} + (1 - y)E_{g-\text{CZTSSe}} - by(1 - y)$, where y is the ratio of [Se]/[S + Se] and b is the specific optical bowing constant which describes the degree of nonlinearity. For the present sample, $y = [\text{S}]/([\text{S}] + [\text{Se}]) = 0.27$, $b = 0.1$ eV according to the theoretical calculations [20] ,thus the $E_{g-\text{CZTSSe}} = 1.35$ eV by solving above equation, which was very close to the experimental value. In addition, Hall measurements results showed that the sample exhibited p-type semiconductor material characteristic. The resistivity, carrier concentration, and Hall mobility were 0.53 Ω cm, 7.9×10^{18} cm^3, and 7.5 cm^2/(Vs), respectively. This result was suitable for CZTSSe thin film as light absorber layer in solar cells.

4 Conclusions

In summary, we prepared the CZTSSe thin film by a simple two-step method. Firstly, Cu–Zn–Sn precursor was deposited by the thermal evaporation system with a single-source. Then, the precursor was annealed in a mixed atmosphere consisting S and Se to form the CZTSSe thin film. The shift of XRD diffraction peaks combined with the two-mode behavior of Raman pattern confirmed the formation of CZTSSe solid solutions. The SEM results showed that the CZTSSe thin film had a uniform morphology and large grains. The optical gap was estimated to be 1.33 eV by UV–Vis transmittance spectrum. Optimal optical and electrical properties indicated that the CZTSSe thin film was promising as an absorber layer in thin film solar cells.

References

[1] K. Ito, T. Nakazawa, Jpn. J. Appl. Phys. **27**, 2094 (1988)

[2] J.S. Seol, S.Y. Lee, J.C. Lee, H.D. Nam, K.H. Kim, Sol. Energy Mater. Sol. Cells **75**, 155 (2003)

[3] D.B. Mitzi, O. Gunawan, T.K. Todorov, K.J. Wang, S. Guha, Sol. Energy Mater. Sol. Cells **95**, 1421 (2011)

[4] T.K. Todorov, J. Tang, S. Bag, O. Gunawan, T. Gokmen, Y. Zhu, D.B. Mitzi, Adv. Energy Mater. **3**, 34 (2013)

[5] J. He, L. Sun, S.Y. Chen, Y. Chen, P.X. Yang, J.H. Chu, J. Alloys Compd. **511**, 129 (2012)

[6] L. Grenet, S. Bernardi, D. Kohen, C. Lepoittevin, S. Noël, N. Karst, A. Brioude, S. Perraud, H. Mariette, Sol. Energy Mater. Sol. Cells **101**, 11 (2012)

[7] P.M.P. Salomé, J. Malaquias, P.A. Fernandes, M.S. Ferreira, A.F. da Cunha, J.P. Leitão, J.C. González, F.M. Matinaga, Sol. Energy Mater. Sol. Cells **101**, 147 (2012)

[8] V. Chawla, B. Clemens, in *Photovoltaic Specialists Conference 38th IEEE*, (Austin Convention Center, Austin, 2012)

[9] J. He, L. Sun, N.F. Ding, H. Kong, S.H. Zuo, S.Y. Chen, Y. Chen, P.X. Yang, J.H. Chu, J. Alloys Compd. **529**, 34 (2012)

[10] M. Grossberg, J. Krustok, J. Raudoja, L. Timmo, M. Altosaar, T. Raadik, Thin Solid Films **519**, 7403 (2011)

[11] Q. Guo, G.M. Ford, W.C. Yang, B.C. Walker, E.A. Stach, H.W. Hillhouse, R. Agrawal, J. Am. Chem. Soc. **132**, 17384 (2010)

[12] W.B. Yang, H.S. Duan, B. Bob, H.P. Zhou, B. Lei, C.H. Chung, S.H. Li, W.W. Hou, Y. Yang, Adv. Mater. **24**, 6323 (2012)

[13] R. Lechner, S. Jost, J. Palm, M. Gowtham, F. Sorin, B. Louis, H. Yoo, R.A. Wibowo, R. Hock, Thin Solid Films **535**, 5 (2012)

[14] N. Momose, M.T. Htay, K. Sakurai, S. Iwano, Y. Hashimoto, K. Ito, Appl. Phys. Exp. **5**, 081201 (2012)

[15] A. Fairbrother, X. Fontané, V. Izquierdo-Roca, M. Espindola-Rodriguez, S. López-Marino, M. Placidi, J. López-García, A. Pérez-Rodríguez, E. Saucedo, Chem. Phys. Chem. **14**, 1836 (2013)

[16] J. Zhang, L.X. Shao, Sci. China Ser. E Technol. Sci. **52**, 269 (2009)

[17] A. Redinger, D.M. Berg, P.J. Dale, S. Siebentritt, J. Am. Chem. Soc. **133**, 3320 (2011)

[18] K.H. Kim, I. Ama, Electron. Mater. Lett. **7**, 225 (2011)

[19] H. Neumann, Helv. Phys. Acta **58**, 337 (1985)

[20] S.Y. Chen, A. Walsh, J.H. Yang, X.G. Gong, L. Sun, P.X. Yang, J.H. Chu, S.H. Wei, Phys. Rev. B **83**, 125201 (2011)